Guardiola, C.; Climent, H.; Pla Moreno, B.; Blanco-Rodriguez, D. (2015). ECU-oriented models for NOx prediction. Part 2: adaptive estimation by using an NOx sensor. Proceedings of the Institution of Mechanical Engineers, Part D: Journal of Automobile Engineering. 229(10):1345-1360. doi:10.1177/0954407014561278.

ECU oriented models for NO_x prediction. Part 2: Adaptive estimation by using a NO_x sensor

C.Guardiola, H.Climent, B.Pla, D.Blanco-Rodriguez

CMT Motores Térmicos, Universitat Politècnica de Valéncia, Camino de Vera s/n, E-46022 Valencia, Spain

Abstract

The implantation of NO_x sensors in diesel engines is necessary in order to track emissions at the engine exhaust for diagnosing and control of the after-treatment devices. However, the use of models is still necessary since the sensor outputs are delayed and filtered. The present paper deals with the problem of the NO_x estimation in two parts, the first part deals with a control-oriented model for the NO_x estimation, while the second part presents data fusion of the model and sensor to improve the estimation, which is presented in the next. The use of models for the NO_x estimation is an alternative but the drift and ageing are still an issue. In order to overcome this problem, the fusion of different signals can be made in a smart way by means of a Kalman filter. There exist different ways of presenting this fusion, from directly tracking the bias to updating the model parameters. According to that, different algorithms are proposed in this paper with the aim of correcting the model output. Furthermore, the estimation of the actual NO_x, by preventing sensor delay and filtering, is also integrated in the algorithm, being a suitable strategy for combining NO_x sensors and models in an on-board basis.

Keywords: NO_x model; Kalman filter; adaptive filtering; data fusion; look-up tables; diesel engine; NO_x sensor; control
PACS: 5.70.a, 89.40.Bb

1. Introduction

Due to the new emission standards, the complexity of the diesel engines is growing and so the number of engine variables to be controlled and supervised. Regarding the NO_x emissions control in light-duty (LD) diesel engines without SCR and LNT (the standard in EURO 5 engines) [1], the engine is calibrated offline before going to market and the parameters in the electronic control unit (ECU) are tuned for fulfilling emissions limits but the emissions are not tracked on-board, i.e. no physical nor virtual sensors are installed in order to track pipe-out emissions.

With regards to the engine calibration, the emissions are usually measured in test rigs with laboratory sensors with limited dynamic capabilities, and the standard procedures are often based on steady-state measurements, with validation in slow dynamic homologation cycles, as the new

Email addresses: carguaga@mot.upv.es (C.Guardiola), hcliment@mot.upv.es (H.Climent), benplamo@mot.upv.es (B.Pla), dablarod@mot.upv.es (D.Blanco-Rodriguez)

European driving cycle (NEDC), which are not representative of real-life driving cycles [2]. Furthermore, this procedure does not ensure that the engine keeps working as when was calibrated.

However, the future dynamic homologation cycles, such as the world light transient cycle (WLTC) or the future real driving emission cycles (RDE), are gradually changing the view of the engine calibration. These cycles present sharper operating point variations, and the dynamic measurement of emissions become necessary, see for example the portable emission measurement systems (PEMS) [3]. Finally, the hardware unit-to-unit dispersion (engine, sensors, etc.), the systems ageing and the effects of other external variables (temperature, pressure, humidity, etc.) are other factors to consider, making that the original calibration cannot fulfil emission targets anymore after a certain mileage. Alternatively, these calibrations are often conservative in order to avoid the engine degradation, and therefore, the fuel penalty is another issue to consider. A clear example is the NO_x control, the engine is forced to work with a certain NO_x security margin with respect to the emission target, making that the engine is not as efficient as it could be. The same occurs with other emissions (PM, HC, CO) and with the CO_2 emissions, even though the industry is pushing the effort in the CO_2 reduction [4], and thus fuel consumption reduction.

In order to monitor the emissions on-board, control oriented models may be used for tracking the emissions [5, 6]; see the part 1 of the paper that presents a control oriented NO_x model. The second part of the paper proposes the installation of an on-board NO_xZrO_2-based sensor [7, 8, 9] at the engine exhaust in order to measure NO_x and fuse this signal with the one of the NO_x model. With respect to the NO_x sensor accuracy, the ZrO_2 sensor can be calibrated by comparing the signal with the one of a gas analyser, used as static standard. A set of steady-state tests already used in part 1 of the paper is utilised here for the sensor calibration, causing NO_x concentration variations to cover the sensor measuring range. Figure 1 illustrates the results. The mean absolute error after calibrating NO_x from ZrO_2 output results is 10.7 ppm, and the residuum standard deviation is 14.77 ppm (see [10] for more information).

Nevertheless, the dynamic response of the sensor is slow and delayed and cannot be used if transient accuracy is necessary. Figure 2 compares the sensor signal (z_{NO_x}) with the response time of the real time NO_x model (x_{NO_x}) described in part 1 of the paper, and it is clear how z_{NO_x} is delayed and filtered with respect to x_{NO_x}. According to [10], where start of injection steps are performed in order to cause sharp NO_x variations, the response time and delay of the sensor is in the order of 1 s.

Data fusion techniques [11, 12] combine different information sources in order to improve the accuracy of the final estimation. In such sense, control oriented models can catch with acceptable precision the transient performance but they are not free from drift and ageing [6, 13]. In order to solve this problem, the fusion of the model signal with the sensor signal can be made in a smart way by means of a Kalman filter (KF) [14, 15], and the model output and parameters might be updated by minimising the estimation error [16, 17]. In this work, two different possibilities for fusion of the NO_x model and sensor signals are proposed:

- Estimation of NO_x by drift correction methods based on an augmented model [18, 19],
- estimation of NO_x by updating look-up tables representing nominal NO_x emissions by means of a computationally efficient KF based method [20]. In this case, two separate applications are proposed: First, a single look-up table is updated online for representing NO_x emissions and second, the main table representing nominal NO_x emissions in the MVEM of the part 1 of the paper is updated by means of fusing the outputs from the sensor and the model.

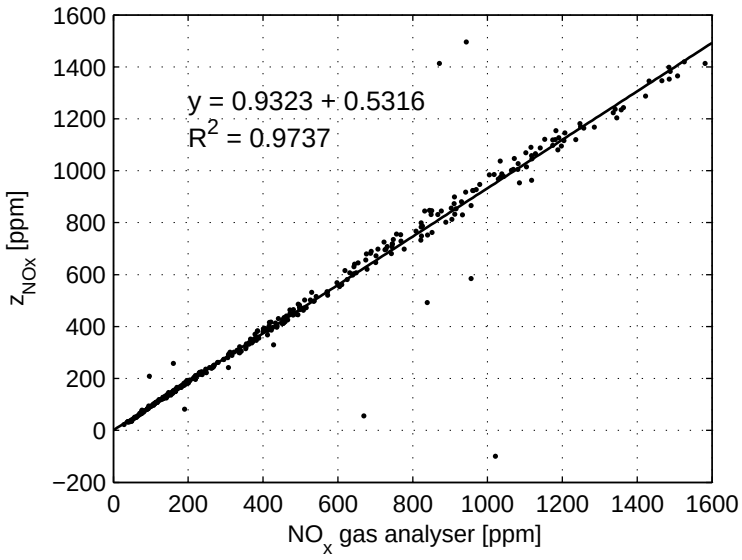

Figure 1: NO_x from ZrO_2 sensor (z_{NO_x}) and the gas analyser under different steady operating conditions; the linear fit and the regression coefficients are represented.

The sensor dynamic response should be characterised in order to give a fast and actual estimation of the considered variable. However, the application of an inverse transfer function [21], once the dynamic characteristics of the sensors are known, does not permit the real time online estimation since the sensor delay cannot be avoided, i.e. the operation is not causal. Admittedly, the sensor dynamic model may be implemented in the fusion algorithms, making possible the tracking of the actual NO_x estimation at the engine exhaust.

This paper is the second part of a work dedicated to show different possibilities for the on-board estimation of NO_x and it presents different adaptive filtering algorithms for estimating NO_x on-board by means of fusing the outputs from a NO_x sensor and a control-oriented NO_x model. In addition, the updating of the NO_x model is discussed. The paper is structured as follows: the section 2 briefly shows the experimental facility with the engine test-bench and measurement equipment (the reader is referenced to the part 1 of the paper [2] for a more complete description); the section 3 briefly describes a real time NO_x model based on a look-up table structure and a number of corrections (see also part 1 of the paper [2] for the complete description); the section 4 presents three different adaptive adaptive filtering algorithms for the NO_x estimation by fusing models and sensors, which are applied in the next sections; the section 5 presents the results of applying the algorithms: updating of look-up tables, updating of the NO_x model and the online observation of the actual NO_x; finally, the section 6 presents the conclusions of this work. The reader is also referenced to the Appendices for finding a list on the acronyms and variables used in this paper as well as other information regarding the engine cycles.

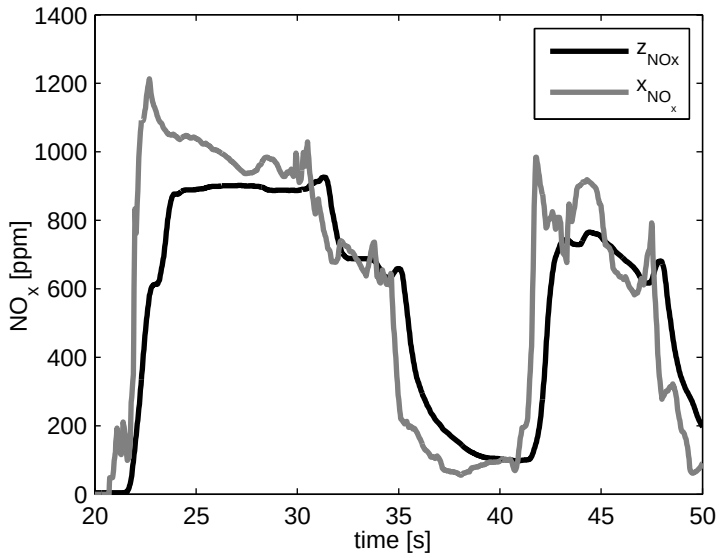

Figure 2: x_{NO_x} and z_{NO_x} in a TRAN A cycle (see part 1 of the paper for the cycles definition). x_{NO_x} is the actual NO_x estimation, no delay nor filtering is expected.

2. Experimental Facility

The experimental data is obtained from a sequential parallel turbocharged diesel engine. This engine is a 2.2-liter 4-cylinder common rail and the specifications are shown in Table 1. The standard air cooler downstream the compressor is replaced by a water intercooler because of the lack of forced air flux. All after-treatment devices are removed, as far as they are out of the scope of the paper. A NO_x sensor, which was used for calibration or comparison in the part 1 of the paper, is installed at the turbine outlet and is now required for implementing the algorithms developed in this paper. This NO_x sensor is also capable of measuring the fuel-to-air ratio or richness. The detailed description of the engine test-bench is skipped and the reader is referred to the part 1 of the paper.

Engine cycles. The algorithms developed in this work are applied to different engine cycles that are summed up in the Table 2. Some of these cycles were already described in the part 1 of the paper: two versions of the FTP 75 cycles for heavy-duty engines and named here as TRAN A and TRAN B (TRAN because of *transient*); the new European driving cycle (NEDC); the urban common Artemis driving cycle (CADC); and a designed sportive driving mountain profile (SDMP). In addition to these, the rural and highway versions of the CADC are also tested (see Appendix C) and the SDMP cycle is repeated two times with minimum variations but similar profiles.

Stroke (S)	96 mm
Bore (D)	85 mm
S/D	1.129
Number of cylinders (z)	4
Displacement	2179 cm^3
Turbocharging system	Sequential parallel [22]
Valves by cylinder	4
Maximum power	125 kW@4000 rpm
Compression ratio	17:1

Table 1: Engine technical data.

Number	Repetitions
TRAN A & B	36 (see part 1 of this paper)
NEDC (warm)	1
Urban CADC	1
Rural CADC	1
Highway CADC	1
SDMP	2 (namely A and B)

Table 2: Description of the engine cycles.

3. A mean value engine model for NO_x prediction

In the first part of the paper, an engine-out NO_x model was designed considering the state vector X

$$X = \begin{bmatrix} x_{NO_x} & y_{NO_x} & C_{dyn} \end{bmatrix}^T \tag{1}$$

where x_{NO_x} is the NO_x model output (actual NO_x), y_{NO_x} is the filtered and delayed NO_x model output (for comparing with NO_x sensor) and C_{dyn} is a dynamic factor for coping with the in-cylinder temperature. The input signals contained in the vector U are standard signals available in the ECU, excepting the humidity where if an appropriate sensor is installed could be included in the model

$$U = \begin{bmatrix} n & m_f & p_{boost} & \dot{m}_a & T_{boost} & T_{cool} & H \end{bmatrix}^T \tag{2}$$

Model output vector Y is the modelled sensor response

$$Y = y_{NO_x} \tag{3}$$

in order to have a comparable signal with NO_x sensor output (z_{NO_x}) during dynamic tests. x_{NO_x} indicates the raw or actual NO_x, which must be filtered and delayed. A delayed first order discrete model is used

$$y_{NO_x} = z^{-\tau_{NO_x}} \frac{1 - a_{NO_x}}{1 - a_{NO_x} z^{-1}} x_{NO_x} \tag{4}$$

where a_{NO_x} is the sensor time response and τ_{NO_x} is the total sensor delay (see [10] for more information about sensor characterisation), while z comes from the Z-Transform.

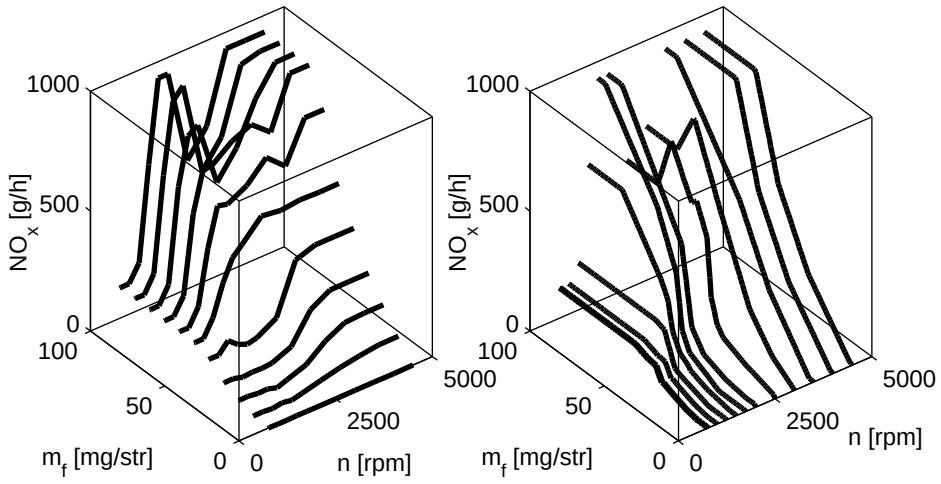

Figure 3: NO_x map plotted in the n and m_f directions. Left plot represents the NO_x emissions at iso-m_f values, while right plot shows the NO_x emissions at iso-n.

The NO_x model main equation is presented in (5) and consists in a single function referenced to conditions with nominal exhaust gas recirculation rate (EGR) for calculating x_{NO_x}, which is affected by an exponential $EGR\lambda^{-1}$ correction for coping with intake oxygen variation and additional factors C_{NO_x} and C_{dyn}[1]. This structure guarantees that nominal tests corrections are eliminated minimising the nominal error and subscript 0 represents the nominal conditions. Then, the model x_{NO_x} output is calculated as follows

$$x_{NO_x} = NO_{x,0} \cdot e^{-k_{NO_x} \cdot (EGR\lambda^{-1} - EGR_0\lambda_0^{-1})} \cdot C_{NO_x} \cdot C_{dyn} \tag{5a}$$

$$C_{NO_x} = C_{\dot{m}_{int}} \cdot C_{T_{int}} \cdot C_{T_{cool}} \cdot C_h \tag{5b}$$

where C_{NO_x} and C_{dyn} are used as correction factors to the model structure.

Figure 3 shows the nominal $NO_{x,0}$ map used for the NO_x model (5). This map is filled with an intensive DOE comprising 363 steady-state tests. The NO_x sensitivity depends on the engine operating point conditions, with a clear difference between the EGR area, transition and areas without EGR. Note that all elements of $NO_{x,0}$ are filled in order to avoid numerical problems, indeed areas that are not reached for the engine (beyond the full load line).

4. Adaptive filtering for predicting NO_x

If a model, with sufficient capacity for reproducing transient NO_x, and a steady-state reliable (although slow) sensor are available on-engine, both information can be fused, by using an extended Kalman filter (EKF) -the non-linear version of the Kalman filter-, in order to get a reliable

[1] λ^{-1} is the relative fuel-to-air ratio or richness.

estimation. In this case, a NO_x sensor and different alternatives for modelling are used in order to estimate NO_x by means of designing three different algorithms based on the EKF:

- Algorithm A: A drift correction algorithm designed in [19] permits to track the bias on the output of a NO_x model presented in [20]. The bias is tracked online but models are not re-calibrated.
- Algorithm B: A single look-up table depending on the engine operating point conditions, speed and injected fuel mass flow under quasi-static assumptions, is updated and used as a model for predicting NO_x. This approach is valid for slow cycles, such as the NEDC[2]. The table is updated by using a simplified Kalman filter (SKF) algorithm, presented in [20].
- Algorithm C: The NO_x model (5) is adapted and re-tuned online by tracking the nominal NO_x. With this strategy, the nominal NO_x map may be fitted by using the dynamic tests, indeed avoiding the steady-state campaign usually needed for the calibration of maps. The state-space system built for the algorithm B is slightly modified in order to consider model parameters. The SKF method is still used for updating the table.

Figure 4 schematises the three options. The objective is on one hand, obtaining a fast and reliable estimation of the NO_x concentration, i.e. without sensor filtering and, on the other hand, introducing adaptive capabilities to models. The methods, although applied to NO_x, could be easily implemented for other relevant variables such as the fuel-to-air ratio (λ^{-1}) or soot.

4.1. Algorithm A: adaptive filtering for correcting drift

Top plot of Figure 4 shows the scheme of a drift correction algorithm, which is well explained in [19]. In general, a linear discrete state-space model is built as follows

$$x_k = Ax_{k-1} + Bu_k + w_k \tag{6a}$$
$$z_k = Cx_k + v_k \tag{6b}$$

where $x_k \in \mathbb{R}^{n_x}$, $u_k \in \mathbb{R}^{n_u}$, $z_k \in \mathbb{R}$ are the state-space, the inputs and the output vectors respectively, while $w_k \sim \mathrm{N}(0,\sigma_w^2)$ and $v_k \sim \mathrm{N}(0,\sigma_v^2)$ are uncorrelated noise applied to the state-vector and output estimation respectively.

The NO_x sensor dynamics are modelled by a first order filter with response time a_{NO_x} and delay τ_{NO_x} [10], where higher order filters maintaining the linear structure might be easily programmed by increasing the state-space order. The discrete equation is defined at a certain time k when considering a given sample time (T_s)

$$x_{NO_x f}(k) = \frac{1 - a_{NO_x}}{1 - a_{NO_x} z^{-1}} x_{NO_x}(k - \tau_{NO_x}/T_s) \tag{7}$$

where $x_{NO_x}(k) \in \mathbb{R}$ is the NO_x model output (see part 1) and $x_{NO_x f}(k) \in \mathbb{R}$ represents the modelled sensor response. In spite of the actual sensor delay is not constant since it is influenced by the transport delay and the sensor non-linear behavior [23], a constant value gives acceptable results for the considered cycles [10]. The response time a_{NO_x} of the sensor is highly constant whatever

[2]The reader is referenced to Section 2.2 of part 1 of the paper [2] for a discussion on the validity of static models for reproducing transient NO_x emissions in cycles.

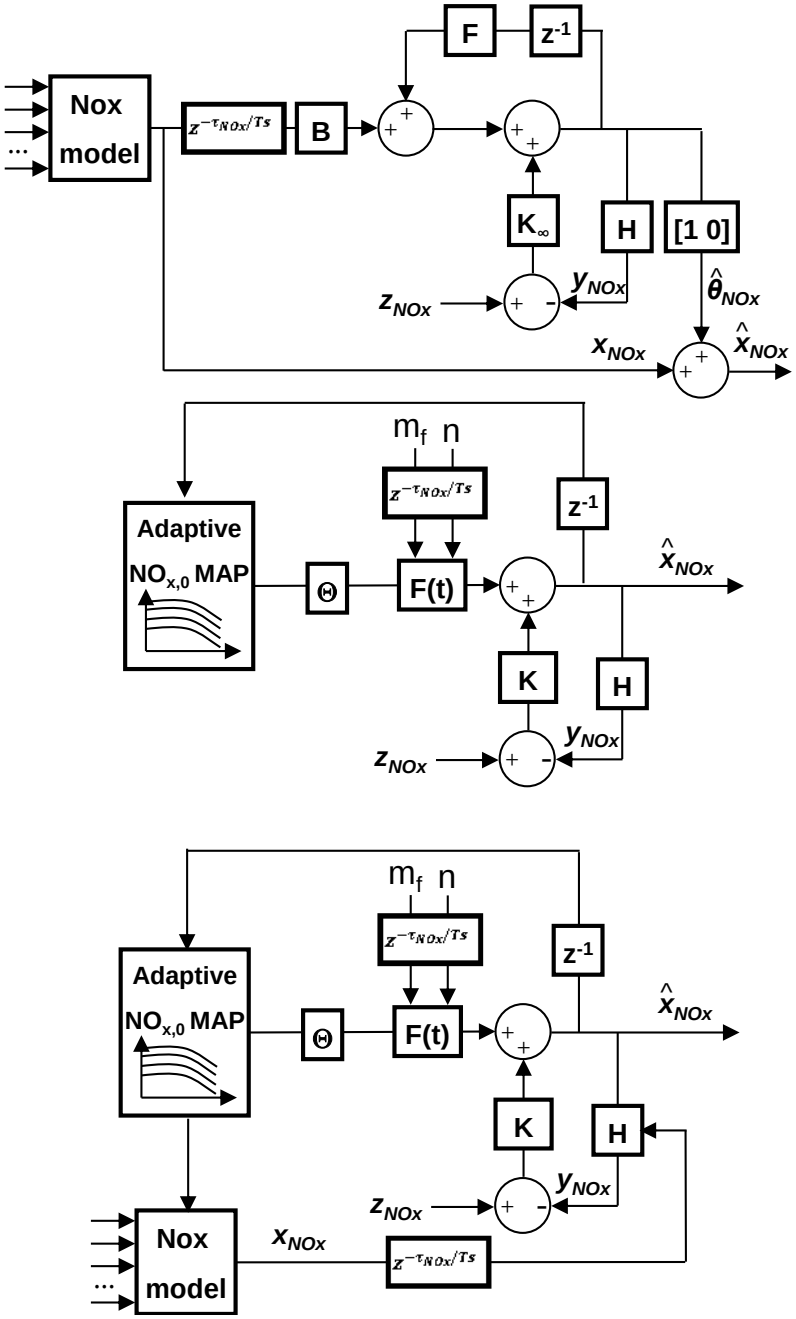

Figure 4: From top to bottom, algorithms A to C: drift correction model, adaptive table for NO_x estimation and adaptive NO_x model.

the conditions. The model and the discussion above can be easily extended to other variables such as λ^{-1} just replacing NO_x by λ^{-1} when it should be necessary.

The bias $\theta_{NO_x}(k - \tau_{NO_x}/T_s) \in \mathbb{R}$ between model and sensor low frequencies is tracked by augmenting the model with an extra-state. Note that T_s is the sampling period and θ_{NO_x} is delayed for coping with sensor delay. Therefore, the state-space model (6) becomes

$$x_k = \begin{bmatrix} 1 & 0 \\ 1 - a_{NO_x} & a_{NO_x} \end{bmatrix} x_{k-1} + \begin{bmatrix} 0 \\ 1 - a_{NO_x} \end{bmatrix} u_k + \begin{bmatrix} w_k \\ 0 \end{bmatrix} \tag{8a}$$

$$z_k = \begin{bmatrix} 0 & 1 \end{bmatrix} x_k + v_k \tag{8b}$$

where vectors are

$$x_k = \begin{bmatrix} \theta_{NO_x}(k - \tau_{NO_x}/T_s) & x_{NO_x f}(k) \end{bmatrix}^T; \quad z_k = z_{NO_x}(k); \quad u_k = x_{NO_x}(k - \tau_{NO_x}/T_s) \tag{9}$$

Now, a steady-state Kalman filter may be designed for observing $\hat{x}_k$

$$\hat{x}_k = A\hat{x}_{k-1} + Bu_k + K_\infty \left(z_{NO_x}(k) - C\left(A\hat{x}_{k-1} + Bu_k\right)\right) \tag{10}$$

and $K_\infty \in \mathbb{R}^n_x$ is the converged steady-state Kalman gain that depends on σ_w^2 and σ_v^2 (see [19]).

4.2. Algorithm B and C: Adaptive filtering for updating tables

Algorithms B and C in Figure 4 are basically methods for updating look-up tables, and these two correspond to two different applications for updating models. Both of them include the learning structure in a state-space model as well as the sensor model, thus providing a systematic and optimal way of manipulating models and maps by means of an observer. The topic of learning look-up tables is treated in the papers [24, 20] and the SKF method presented in [20] is utilised in this work for updating the look-up tables.

Algorithm B updates a map for inferring NO_x while algorithm C updates the main table $NO_{x,0}$ of the NO_x model (5), but both deals with updating a reference map for NO_x. The table elements are treated as states and their variation is supposed slow and only driven by the existing noise. The general state-space model for updating look-up tables is then as follows

$$x_k = F_k x_{k-1} + w_k \tag{11a}$$

$$y_k = H_k x_k + v_k \tag{11b}$$

with matrices and noise vectors fulfilling properties of the linear state-space model (6) but now coping with the time and state dependence, i.e. F_k and H_k may vary with time.

The main difference between both approaches is that the Observer C also considers the dynamics and NO_x model parameters. Anyhow and independently of using a single table or the NO_x model, the updating procedure is similar: the problem consists on updating a 2D look-up table $\mathbf{\Theta}_{NO_x} \in \mathbb{R}^{n_1 \times n_2}$, which is scheduled here by the engine speed (n) and the injected fuel mass flow[3] ($\dot{m}_f$). In the next, the interpolation of the look-up table and the updating procedure are presented.

[3]Note that engine torque or mean effective pressures could be used instead of $\dot{m}_f$ for representing the engine load.

4.2.1. Representation and interpolation of 2D maps

Mathematically, $\mathbf{\Theta}_{\mathrm{NO_x}}$ represents a vectorial transformation $\{n, \dot{m}_f\} \rightarrow x_{\mathrm{NO_x}}$ whose elements are $[\mathbf{\Theta}_{ij}]$ and the output is computing by a 2D linear interpolation

$$x_{\mathrm{NO_x}} = \mathrm{vec}\left(q(n(k), m_f(k))\right)^T \mathrm{vec}(\mathbf{\Theta}_{\mathrm{NO_x}}) \tag{12}$$

where $vec(\cdot)$ is the vectorial transformation and q the interpolation matrix

$$\begin{bmatrix} q_{i,j}(k) & q_{i,j+1}(k) \\ q_{i+1,j}(k) & q_{i+1,j+1}(k) \end{bmatrix} = \begin{bmatrix} (1-\eta_1(k))(1-\eta_2(k)) & (1-\eta_1(k))\eta_2(k) \\ \eta_1(k)(1-\eta_2(k)) & \eta_1(k)\eta_2(k) \end{bmatrix}$$

with

$$\eta_1(k) = \frac{n(k - \tau_{\mathrm{NO_x}}/T_s) - r_i}{r_{i+1} - r_i}, \qquad \eta_2(k) = \frac{m_f(k - \tau_{\mathrm{NO_x}}/T_s) - c_j}{c_{j+1} - c_j} \tag{13}$$

$r \in \mathbb{R}^{n_1}$ and $c \in \mathbb{R}^{n_2}$ represent the grids on n and m_f respectively (r stands for row and c for column). See also how n and m_f are conveniently delayed for coping with the sensor lag.

Finally, $x_{\mathrm{NO_x}}$ is the map output.

$$x_{\mathrm{NO_x}}(k - \tau_{\mathrm{NO_x}}/T_s) = \mathrm{vec}\left(q(u_k)\right)^T \mathrm{vec}(\mathbf{\Theta}_{\mathrm{NO_x}}) \tag{14}$$

The map output is conveniently filtered (note that map inputs have already been delayed) for comparing with the sensor signal $z_{\mathrm{NO_x}}$.

$$y_{\mathrm{NO_x}} = \frac{1 - a_{\mathrm{NO_x}}}{1 - a_{\mathrm{NO_x}} z^{-1}} x_{\mathrm{NO_x}} \tag{15}$$

4.2.2. Updating look-up tables

The state vector for the model (11) is built with $vec(\mathbf{\Theta}_{\mathrm{NO_x}})$ and the extra-state $x_{\mathrm{NO_x}f}(k)$ for capturing the sensor behavior with a first order filter

$$x_k = \begin{bmatrix} vec(\mathbf{\Theta}_{\mathrm{NO_x},\mathbf{k}}) & x_{\mathrm{NO_x}f}(k) \end{bmatrix}^T \tag{16}$$

F_k is

$$F_k = \left[\begin{array}{c|c} \multirow{4}{*}{$\mathbf{I_4}$} & \begin{matrix}0\\0\\0\\0\end{matrix} \\ & \\ & \\ & \\ \hline (1-a_{\mathrm{NO_x}})q_k & a_{\mathrm{NO_x}} \end{array}\right] \tag{17}$$

I is the unitary matrix and consequently, the variance matrix Q_k of noise vector w_k is

$$\mathbf{Q_k} = \left[\begin{array}{c|c} \mathbf{Q} & \mathbf{0} \\ \hline \mathbf{0} & \sigma_f^2 \end{array}\right] \tag{18}$$

where σ_f^2 is the variance of the noise applied to the sensor model, while

$$\mathbf{Q} = \begin{bmatrix} \sigma_w^2 & & & \\ & \sigma_w^2 & & \\ & & \ddots & \\ & & & \sigma_w^2 \end{bmatrix} \tag{19}$$

which is consistent with considering that the noise linked to the map elements is uncorrelated and constant; i.e. $w_k \sim \mathrm{N}(0,\sigma_w^2)$, and the same for all elements. If there is enough engineering information, the variances at every element state might be considered different.

In the case of the observer B, the output matrix

$$H = [zeros(length(vec(\mathbf{\Theta}_{\mathrm{NO_x}}))) \quad 1] \tag{20}$$

is constant and just acts as a selector of the state $x_{\mathrm{NO_x}f}(k)$ for comparing with sensor. However, if the table of a dedicate model is updated, H_k should be arranged in order to cope with model equation, as explained after in Section 5.2.

Therefore, the updating problem is solved by observing $\hat{x}$ with an EKF

$$\hat{x}_k = F_k\hat{x}_{k-1} + K_k\left(z_{\mathrm{NO_x}}(k) - H_k\left(F_k\hat{x}_{k-1}\right)\right) \tag{21}$$

where K_k depends on F_k, H_k and the noise selection $(\sigma_w^2, \sigma_f^2, \sigma_v^2)$. For this problem, the standard EKF gives the iterative solution for obtaining K_k as shown in [17] but due to the big computational resources required and the complexity of the computing, a computationally efficient version of the KF, namely simplified KF (SKF) and published in [20], is implemented. The results are similar to those of the EKF but with a much lower computational effort[4].

5. Results

This section presents the results on the application of the different algorithms presented before for the estimation of $\mathrm{NO_x}$: the online updating of look-up tables, the updating of the $\mathrm{NO_x}$ model, and the online observation of the actual $\mathrm{NO_x}$, i.e. by removing the sensor delay and filtering.

5.1. Online updating of look-up tables for modeling NO_x

Following the discussion made in the part 1 of the paper, a single look-up table may represent the engine $\mathrm{NO_x}$ concentration when the changes in both n and $\dot{m}_f$ are slow enough for not compromising the quasi-static hypothesis and the air path control references, namely air mass flow ($\dot{m}_a$) and boost pressure (p_{boost}), are tracked relatively fast, as it is the case of the NEDC.

In these cases, $\mathrm{NO_x}$ can be modelled by using a single 2D adaptive look-up table function of n and m_f whose parameters are estimated with the updating methods. The state-space model (11) is used for updating the table with the algorithm B presented in Figure 4.

Table elements are estimated online while the engine is running without any special calibration procedure or test rig, beyond the availability of an on-board $\mathrm{NO_x}$ sensor. The first time that the engine is running, the parameters are updated, and when the engine switches off, the stored parameters can be used for predicting $\mathrm{NO_x}$. When the engine is running again, the parameters keep evolving for correcting the drift and/or slowly varying effects. Furthermore, the observer built for the map updating can be utilised for having an actual $\mathrm{NO_x}$ estimation as it will be explained in Section 5.3, i.e. avoiding filtering and delay of the sensor.

With respect to the dimensions of the maps used for the adaptive estimation of $\mathrm{NO_x}$ and according to the authors experience, usual dimensions for look-up tables in production engines are between 200 and 400 parameters. The selection of the appropriate dimensions is a trade-off

[4]The paper[20] makes a dedicate comparison between using the SKF and the EKF, as well as other simplified versions based on the EKF.

between the accuracy and the computational resources. An excessive density can compromise the table convergence, requiring more filtering and excitation, but a higher density of scheduling points can also improve the accuracy of the solution.

The grid used in this work for the observation is defined as follows

$$c = [0:5:30 \quad 34:4:50 \quad 55:5:80] \tag{22a}$$

$$r = [750 \quad 1000 \quad 1250 \quad 1500 \quad 1750 \quad 2000:500:4500] \tag{22b}$$

where c represents the grid for m_f [mg/str] and r for n [rpm], building a matrix with 198 elements (11×18)

Filter design. The state-space model (11) is built with the following numerical values

$$a_{\mathrm{NO_x}} = 0.96; \quad \tau_{\mathrm{NO_x}} = 0.75\mathrm{s} \tag{23}$$

while the sampling frequency is 50 Hz ($T_s = 20$ms). Sensor parameters are fitted by performing start of injection (SOI) steps as in [10]. The state-space model output $z_{\mathrm{NO_x}}$ is given by the $\mathrm{NO_x}$ sensor, while inputs are

$$u_{1,k} = \mathrm{z}^{-\tau_{\mathrm{NO_x}}/T_s}\, n(k) \tag{24a}$$

$$u_{2,k} = \mathrm{z}^{-\tau_{\mathrm{NO_x}}/T_s}\, m_f(k) \tag{24b}$$

and the state vector x is

$$x_k = [vec(\mathbf{\Theta}_{\mathrm{NO_x}}) \quad x_{\mathrm{NO_x}f}]^T \tag{25}$$

where $\mathbf{\Theta}_{\mathrm{NO_x}}$ is the table to be updated.

The filter is tuned with the values

$$\sigma_v^2 = 25^2;\ \sigma_w^2 = 7^2;\ \sigma_f^2 = 50^2 \tag{26}$$

Results with engine cycles. The SDMP is a test with sharp variations on the operating point conditions but homologation cycles, such as the NEDC, are much slower. This could compromise the global observability since higher levels of excitation are beneficial for updating. In this cycle, the air path dynamics are fast enough, then $\dot{m}_a$ and p_{boost} are able to track the set-points fixed by the engine calibration according to the engine speed and load. In such case, the use of a look-up table for modelling $\mathrm{NO_x}$ is valid and the table $\mathbf{\Theta}_{\mathrm{NO_x}}$ might directly replace nominal $\mathrm{NO_{x,0}}$ table in the RT $\mathrm{NO_x}$ model. Despite $\mathrm{NO_{x,0}}$ could be used for initializing $\mathbf{\Theta}_{\mathrm{NO_x}}$, here the null matrix is the initial map, which is a worst-case condition.

The NEDC is run for updating $\mathbf{\Theta}_{\mathrm{NO_x}}$ according to the reference $\mathrm{NO_x}$ values at every operating point. After using an adaptive map and the SKF method with the calibration (26), the results are shown in Figure 5. There, $y_{\mathrm{NO_x}}$ is calculated on the basis of a table $\mathbf{\Theta}_{\mathrm{NO_x}}$ which has been updated according to algorithm B; see (21). The $\mathrm{NO_x}$ estimation by the adaptive map is able to reproduce the sensor output $z_{\mathrm{NO_x}}$ after updating the table.

In the case of a fast cycle, e.g. the SDMP, the EGR valve is closed the most of the time. Therefore, $\mathrm{NO_x}$ is function only of n and m_f when the EGR valve is closed, but keeping in mind that engine settings do not correspond with the nominal steady-state settings (since the EGR valve would not be closed)

$$x = f(n, m_f, m_a^*(n, m_f), p_b^*(n, m_f))_{u_{\mathrm{egr}}=0} = f(n, m_f)_{u_{\mathrm{egr}}=0} \tag{27}$$

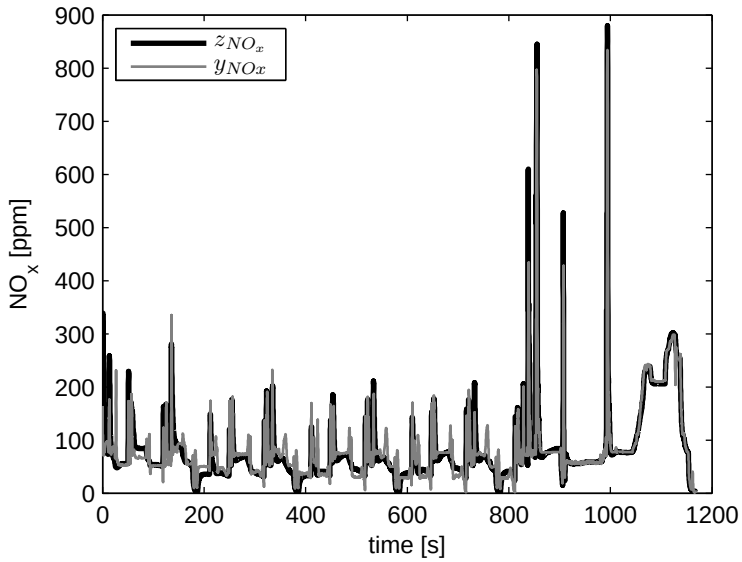

Figure 5: Adaptive NO_x estimation in the NEDC, where it is estimated with a table that is updated during the whole cycle and then used for simulating y_{NO_x}. z_{NO_x} is provided for comparison.

In the case of the NEDC or CADC cycles, transients are much slower and the engine works closer to the nominal settings. In such case, states are also function of n and m_f but for nominal operation of EGR-VGT controller. Possible states can now be approximated with

$$x = f(n, m_f, m_a^*(n, m_f), p_b^*(n, m_f))_0 = f(n, m_f)_0 \tag{28}$$

Figure 6 shows the predicted NO_x emissions in the cycle SDMP B (top plot) and NEDC (bottom plot) after using an updated map $\mathbf{\Theta}_{NO_x}$ in another repetition of the cycle SDMP A (different from the previous one). The table output is filtered and delayed by a sensor model with the parameters $a = 0.96$ and $\tau = 0.75$s. The ability to reproduce NO_x on SDMP is clear while a bias exists in the NEDC. Nevertheless, NO_x estimation during urban part is not as bad as in the highway part, where NO_x is overestimated as expected ($\mathbf{\Theta}_{NO_x}$ has been fitted with nearly zero EGR conditions).

However, if updating $\mathbf{\Theta}_{NO_x}$ with the NEDC cycle and then using the results for predicting the SDMP B, shown in top plot of Figure 7, the results are quite bad as a big area of the engine map is not covered and active areas present lower NO_x emissions because of the EGR actuation. The prediction using $\mathbf{\Theta}_{NO_x}$ in the CADC urban cycle is quite better even though not perfect, as covered areas are similar. Anyway, the use of adaptive maps could be useful when the operating point variations do not vary rapidly, since it occurs with the NEDC.

5.2. Online updating of the NO_x model

The SKF could be applied to the online adaptation and/or calibration of complex models, where a number of maps and parameters must be updated. Admittedly, a deep study is required for ensuring observability, convergence and robustness properties and for getting a computationally efficient learning structure, i.e. a big number of parameters and maps should be updated and

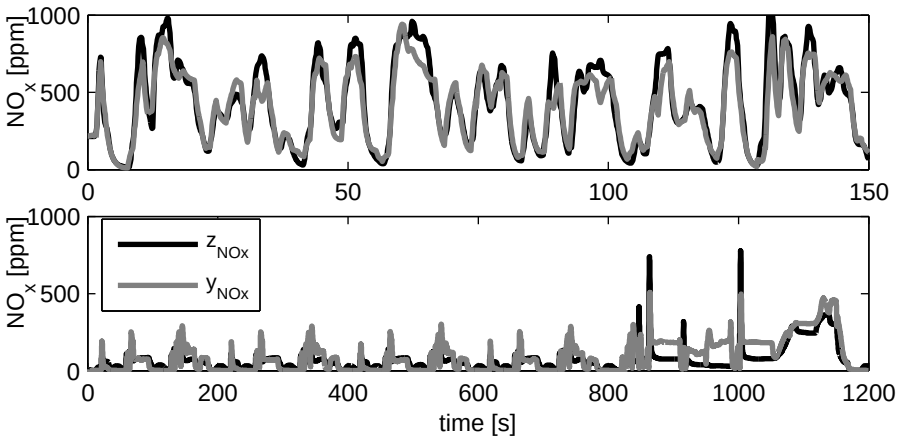

Figure 6: Offline NO_x prediction y_{NO_x} compared with the NO_x sensor z_{NO_x} by using a table $\mathbf{\Theta}_{NO_x}$ updated online with the SDMP A cycle. Top plot: results in SDMP B cycle. Bottom plot: results in NEDC cycle. The legend is valid for both plots.

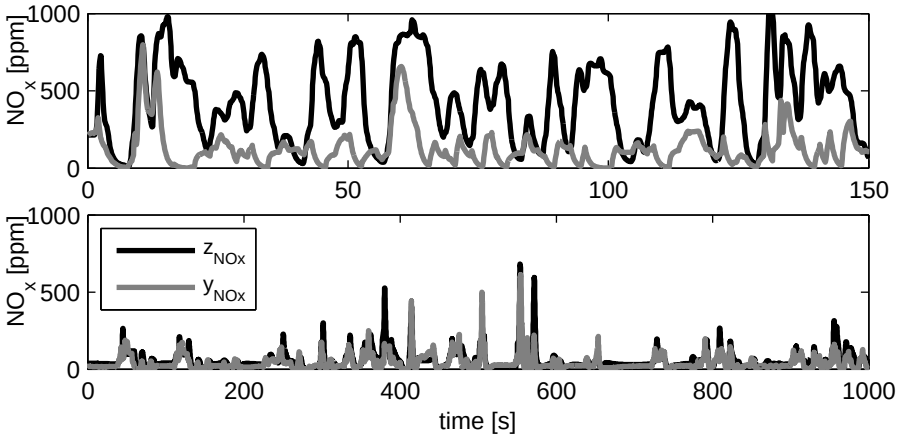

Figure 7: Offline NO_x prediction y_{NO_x} compared with the NO_x sensor z_{NO_x} by using a table $\mathbf{\Theta}_{NO_x}$ updated online with the NEDC cycle. Top plot: results in SDMP B cycle. Bottom plot: results in CADC urban cycle. The legend is valid for both plots.

the problem is non-convex. However, some model parameters or indeed inputs can be updated independently by means of designing an appropriate observer.

In this section, adaptive capabilities are proved in the NO_x model (5) [25], and the state-space vector X could be augmented as follows

$$X = \begin{bmatrix} x_{NO_x} & y_{NO_x} & x_\lambda^{-1} & y_\lambda^{-1} & vec(\mathbf{\Theta}_{NO_x}) & \theta \end{bmatrix}^T \tag{29}$$

where besides x_{NO_x} and y_{NO_x}[5]; λ^{-1} (used as input for the RT NO_x model), the nominal NO_x map $\mathbf{\Theta}_{NO_x}$ and the model bias θ could be included.

On one side, the use of an observer for λ^{-1} if the NO_x sensor is available is completely justified due to the NO_x sensitivity to errors on mistaking intake oxygen [26]. Furthermore, the error sources in the λ^{-1} model are well explained in [19], namely drift on the estimated $\dot{m}_f$ by the ECU and/or drift on sensor $\dot{m}_a$ signal. Figure 8 precisely compares the model output y_{NO_x} when a drift on x_λ^{-1} occurs. Here, the top plot compares richness output ($z_{\lambda^{-1}}$) given by the NO_x sensor, x_λ^{-1} from a model

$$x_\lambda^{-1} = 14.5\frac{\dot{m}_f}{\dot{m}_a} \tag{30}$$

and the observation $\hat{x}_{\lambda^{-1}}$ by a KF, when a clear drift on x_λ^{-1} exists [6] [19]. If the drifted signal is used for inferring NO_x by the model, the output is also drifted from the sensor signal as shown in bottom plot. However, if observing $\hat{x}_{\lambda^{-1}}$ by a KF, the NO_x output keeps the model accuracy. Therefore, the benefits of observing λ^{-1} by a KF are clear.

Learning algorithm for updating NO_x model. At the same time, model errors and ageing can be corrected online by tracking the bias as in algorithm A, or by observing the nominal $NO_{x,0}$ table for also improving the prediction capabilities of the model. The former is useful for the actual NO_x prediction as discussed in the next subsection, while the latter is advisable for correcting model ageing as presented in the next.

The state-space vector

$$X^w = \begin{bmatrix} x_{NO_x} & y_{NO_x} & x_\lambda^{-1} & y_\lambda^{-1} & vec(\mathbf{\Theta}_{NO_x}) \end{bmatrix}^T \tag{31}$$

is built for designing an algorithm like C (see Figure 4) in order to adapt the nominal NO_x table to possible changes in the NO_x emissions, mainly due to ageing. Nevertheless, this structure is useful not only for learning $NO_{x,0}$

$$\mathbf{\Theta}_{NO_x} = NO_{x,0}$$

but for fitting a table without initial knowledge. Depending on the model and sensor uncertainties, the strategy of the filter tuning can be conservative (slow corrections) or aggressive (fast corrections).

The state-space model is similar to that of (11) and also utilised for the algorithm B, but including NO_x model variations and corrections around the nominal values (5) in the output matrix H_k

$$H_k = [zeros(length(vec(\mathbf{\Theta}_{NO_x}))) \quad C_{mod}] \tag{32}$$

[5]Here y_{NO_x} is included in the state-space model instead of $x_{NO_x f}$ for making direct reference to the NO_x model output (5)

[6]Drift on x_λ^{-1} is caused due to failures in air mass flow or injected fuel rate signals, that at the same time will affect EGR flow model and the look-up tables interpolation. In those cases, the sensor signal $z_{\lambda^{-1}}$ can be used for correcting errors on the air mass flow and/or injected fuel rate signal. In this work, the error is only considered in the x_λ^{-1} model.

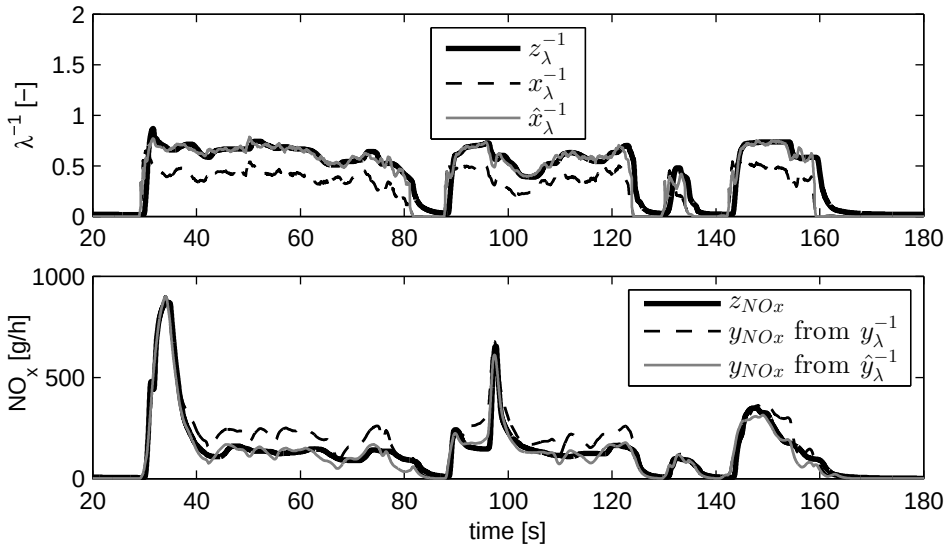

Figure 8: λ^{-1} and NO_x estimations in the TRAN B30 cycle (see part 1 of the paper). Top plot: $z_{\lambda^{-1}}$ sensor signal, x_λ^{-1} calculated by the model and $\hat{x}_{\lambda^{-1}}$ observed by a drift augmented model. Bottom plot: NO_x estimation by three ways, z_{NO_x} sensor signal, y_{NO_x} by the NO_x model using x_λ^{-1} as input and y_{NO_x} by using an adaptive model with $\hat{x}_{\lambda^{-1}}$ as λ^{-1} input.

where

$$C_{mod} = e^{-k_{NO_x} \cdot (EGR\lambda^{-1} - EGR_0\lambda_0^{-1})} \cdot C_{NO_x} \cdot C_{dyn}$$

Other model maps and parameters, such as the volumetric efficiency (η_v) used for calculating the EGR mass flow, might be updated by just applying an EKF similar to that for $NO_{x,0}$ (with the correspondent linearisation). If a full adaptive model is proposed, in a way that all model parameters are affected by noise, then the learning structure lacks of robustness and is difficult to discriminate the observed error between all tables, curves and coefficients. An alternative strategy is observing a drift θ and afterwards weighting the error between model parameters by LS or other strategies [27]. The main limitations are the lack of awareness in the error sources and the limited computational and memory resources existing in the ECU, making inadvisable to design an strategy based on the together updating of all model parameters and tables.

Coming back to the application, $\mathbf{\Theta}_{NO_x}$ is designed with the grid defined by (22) and is updated with the SKF method. The RT NO_x model is simulated with the engine cycles and the errors are computed. Due to system ageing, model is drifted. The SKF method is also used for updating $NO_{x,0}$ coming from the NO_x model and thus correcting drift. The updated model is simulated in those cycles and new errors are computed.

For the given application, z_{NO_x} sensor output is converted from ppm to g/h

$$\dot{x}_{NO_x}^{g/h} = 0.001587 x_{NO_x}^{ppm} \cdot (\dot{m}_a^{kg/h} + \dot{m}_f^{kg/h}) \tag{33}$$

since $NO_{x,0}$ elements units are also g/h.

The noise calibration is adjusted by trial and error and is not guaranteed to be the optimised one

$$\sigma_v^2 = 1;\ \sigma_w^2 = 0.01;\ \sigma_f^2 = 1 \tag{34}$$

while the rest of parameters are suited as in Section 4.

The cycles are tested by maintaining the calibration (34), and the offline NO_x prediction is calculated just after finishing the cycle by using the updated $NO_{x,0}$ in the NO_x model. The computed errors are compared with the ones of the original model output. In these simulations, the initial matrix is the $NO_{x,0}$ map fitted in the part 1 for the NO_x model. Figure 9 shows the results on 4 different cycles, where the original and updated y_{NO_x} are compared with the sensor signal z_{NO_x}. y_{NO_x} with the original calibration presents a bias with respect to z_{NO_x} that is decreased after running the cycles with the SKF.

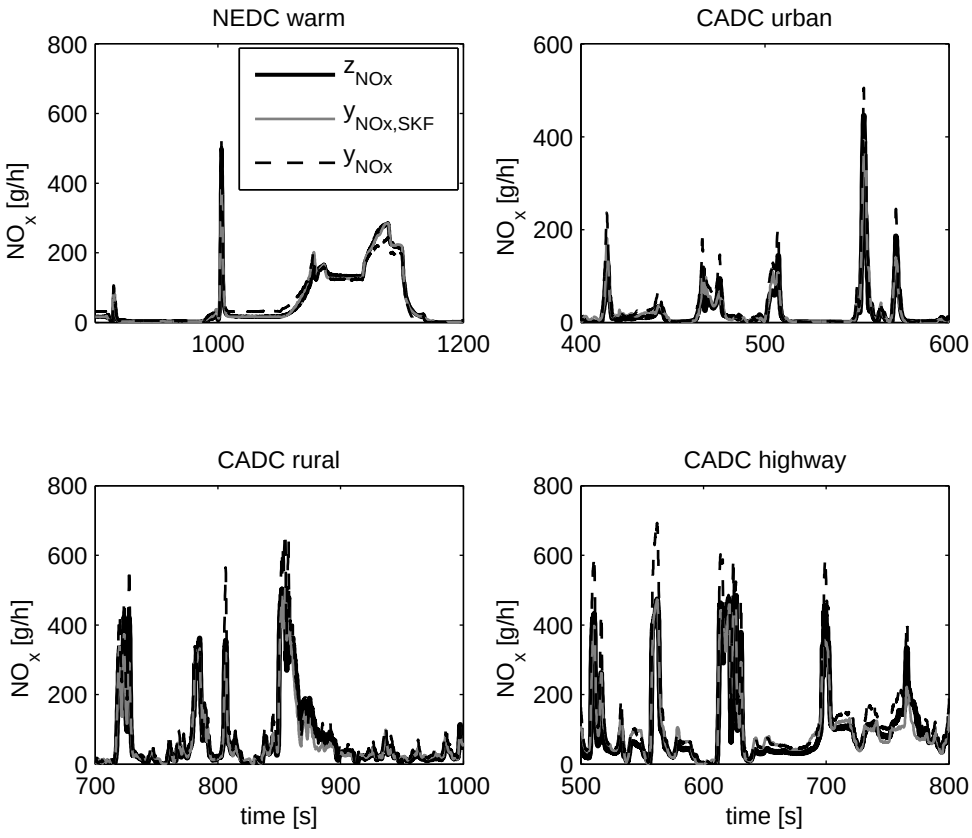

Figure 9: Comparison of NO_x estimation by three different sources: sensor signal z_{NO_x}, y_{NO_x} computed by updating the $NO_{x,0}$ table with the SKF method ($y_{NO_x,SKF}$), and y_{NO_x} by using the RT NO_x model without updating.

Cycle	Model error [g/h]	Updated Model error [g/h]
NEDC	6.14	3.08
CADC Urban	6.40	3.75
CADC Rural	14.81	10.46
CADC Highway	36.23	22.51
SDMP A	49.46	49.13
SDMP B	46.34	43.64

Table 3: Mean absolute errors (g/h) in NO_x output by different estimations. Model column lies on the model error and Updated lies on using the table learnt just after finishing every cycle.

Table 3 compares the absolute mean errors

$$e = mean(\sum z_{NO_x} - y_{NO_x}) \tag{35}$$

by means of simulating the original model output and the adaptive model. The errors are minimised achieving quite better results when updating the model. These results prove the validity of the algorithm and the capabilities for updating models.

With respect to the filter tuning, it has not been optimised for obtaining the results, and a trial-and-error method was followed. Further improvements are in the line of optimising the filter tuning with statistical methods or improving the sensor model, e.g. variable delay. Anyway, the results show the potential of the method for updating models with and without any initial information at all.

5.3. Online observation of the actual NO_x

In the previous subsections, the algorithms were applied in order to update a NO_x model by comparing with the sensor signal, and the final estimations fit the NO_x sensor and not directly the actual NO_x emissions, i.e. without the sensor delay and filtering. In this section, the state vector is augmented with an extra-state for representing actual NO_x. The actual NO_x estimation is advisable for real time purposes, such as real time NO_x control or diagnosis, or for using in the test rig for reconstructing actual NO_x emissions when a fast measurement system is not available, provided that a dynamic model of the sensor is previously identified.

One of the important problems is the causality of the solution since the sensors measure in a delayed basis, mainly due to the transport and hardware delay itself. In the case of the NO_x sensor, this delay cannot be neglected since it is in the order of 1s. To overcome this problem, two possibilities are designed: tracking the bias for the online estimation (algorithm A) and the use of a model learning structure (algorithm C). Both possibilities are based on the ageing cancellation by means of adaptive filtering and are presented in the next.

Actual NO_x by drift correction models. The following state-space vector is built

$$X = \begin{bmatrix} \theta_{NO_x} & x_{NO_x} & x_{NO_x f} \end{bmatrix}^T \tag{36}$$

where x_{NO_x} represents the actual NO_x. The state-space input $u_k = x_{NO_x}(k - \tau_{NO_x}/T_s)$ is conveniently delayed and $z_k = z_{NO_x}$. Matrices $\mathbf{F}$, B and H are modified accordingly

$$\mathbf{F} = \begin{bmatrix} 1 & 0 & 0 \\ 1 & 0 & 0 \\ 0 & 1 - a_{NO_x} & a_{NO_x} \end{bmatrix} \quad B = \begin{bmatrix} 0 \\ 1 \\ 1 - a_{NO_x} \end{bmatrix} \quad H = \begin{bmatrix} 0 & 0 & 1 \end{bmatrix} \tag{37}$$

However and due to the sensor delay, the bias $\hat{\theta}_{\mathrm{NO_x}}(k - \tau_{\mathrm{NO_x}}/T_s)$ at the instant k is observed with a certain delay $\tau_{\mathrm{NO_x}}$, while the actual $\mathrm{NO_x}$ estimation should be

$$\hat{x}_{\mathrm{NO_x}}(k) = x_{\mathrm{NO_x}}(k) + \hat{\theta}_{\mathrm{NO_x}}(k) \tag{38}$$

which corresponds to a non-causal transformation since at a given time, the delayed bias $\theta_{\mathrm{NO_x}}(k - \tau_{\mathrm{NO_x}}/T_s)$ is only available:

$$\hat{x}_{\mathrm{NO_x}}(k) = x_{\mathrm{NO_x}}(k) + \hat{\theta}_{\mathrm{NO_x}}(k - \tau_{\mathrm{NO_x}}/T_s) \tag{39}$$

This calculation could lead to important errors when sharp load transients occur. Alternatively, an adaptive map $\mathbf{\Theta}_{\mathrm{NO_x}} \in \mathbb{R}^2 : n, m_f \rightarrow \theta_{\mathrm{NO_x}}$ might be introduced for modelling drift as a function of the operating point conditions in a similar way as the algorithm B does. This option is well described in [19]: a map is adapted by means of a steady-state version of a KF (similar to a RLS filtering) to store the bias of a λ^{-1} model depending on the operating point conditions. This map is interpolated for giving an initial estimate in the prediction of the state at every iteration. This algorithm might be applied to the $\mathrm{NO_x}$ estimation as follows

$$\hat{x}_k = \mathbf{F}\mathbf{\Theta}_{\mathrm{NO_x},\mathbf{k}}(n(k), m_f(k)) + Bu_k + K_\infty \left(z_{\mathrm{NO_x}}(k) - H\left(\mathbf{F}\hat{x}_{k-1} + Bu_k\right)\right) \tag{40}$$

which is indeed the same observer as the algorithm A presented in the paper with the introduction of an adaptive table $\mathbf{\Theta}_{\mathrm{NO_x}}$, which is updated independently with the algorithm B.

$$\mathbf{\Theta}_{\mathrm{NO_x},\mathbf{k}} = f\left(\mathbf{\Theta}_{\mathrm{NO_x},\mathbf{k-1}}, \hat{x}_k, z_{\mathrm{NO_x}}(k)\right) \tag{41}$$

For the RT estimation, the map itself is interpolated for inferring $\theta_{\mathrm{NO_x}}$ avoiding the causal problem and huge integrations when the drift varies with operating point conditions and time. The final estimation is then calculated as follows

$$\hat{x}_{\mathrm{NO_x}}(k) = x_{\mathrm{NO_x}}(k) + \mathbf{\Theta}_{\mathrm{NO_x},\mathbf{k}}(n(k), m_f(k)) \tag{42}$$

where $\mathbf{\Theta}_{\mathrm{NO_x}}$ refers to a map that stores the $\mathrm{NO_x}$ model bias. This system should solve two different algorithms, one for tracking the bias and the other for updating the table, but it makes possible to separate the problems and apply different algorithms for the two problems. This has the benefit that both problems might be considered as steady-state filters under certain assumptions [24, 19], which further simplifies the calculation since the Kalman gain K_∞ converges.

Actual NO_x by updating look-up tables. The state-space model for learning maps is useful not only for calibrating the map but also for real time observation of $\mathrm{NO_x}$ signal. Therefore, the matrices and the state vector are augmented for introducing $x_{\mathrm{NO_x}}$

$$x_k = \begin{bmatrix} vec(\mathbf{\Theta}_{\mathrm{NO_x}}) & x_{\mathrm{NO_x}}(k) & x_{\mathrm{NO_x}f} \end{bmatrix}^T \tag{43}$$

Now, the local observable matrix $\mathbf{F_k^o}$ is not constant anymore and its variation should be calculated at every iteration

$$\mathbf{F_k^o} = \left[\begin{array}{c|cc} & 0 & 0 \\ \mathbf{I_{4\times 4}} & 0 & 0 \\ & 0 & 0 \\ & 0 & 0 \\ \hline C_{mod} \times q_k & 0 & 0 \\ 0 & (1 - a_{\mathrm{NO_x}}) & a_{\mathrm{NO_x}} \end{array}\right] \tag{44}$$

For the case of the algorithm B for updating only look-up tables, $C_{mod} = 1$. For the case of an algorithm like C and for the NO_x model,

$$C_{mod} = e^{-k_{NO_x} \cdot (EGR\lambda^{-1} - EGR_0\lambda_0^{-1})} \cdot C_{NO_x} \cdot C_{dyn} \tag{45}$$

which it is pre-calibrated offline. Finally, H is now constant for both algorithms B and C.

$$H = [0 \quad 0 \cdots 1] \tag{46}$$

Results. The use of both methods leads to similar results. the look-up tables structure is beneficial as far as can be applied also for updating the model while the drift correction algorithms are not subjected to a model structure (the map interpolation) and can provide a direct bias estimation. The application of the methods in the same state-space structure is possible and presents important advantages, especially when considering the filter tuning. A drift correction method permits to directly track the bias and therefore, the filter should be relatively fast; while the algorithm for updating look-up tables also corrects the bias by improving the model estimation and a relatively slow correction should be advisable for the sake of the robustness. Anyway, as far as the error in the model output is minimised, the identified bias is lower, being zero when the model presents no error at all. The new state-space vector might be built as follows

$$x_k^w = [vec(\mathbf{\Theta}_{NO_x}) \quad \theta_{NO_x} \quad \mathbf{x}_{NO_x}(\mathbf{k}) \quad \mathbf{x}_{NO_x\mathbf{f}}]^T \tag{47}$$

where the four elements represent the look-up table elements, the bias, the actual NO_x and the sensor model estimation respectively, while *w* stands for *wide*.

The model with the state-space vector (43) is observed in order to show an application example of the fast estimation of the actual NO_x. Figure 10 shows results in the cycle SDMP A, by fitting the $NO_{x,0}$ map from the NO_x model (4) with initial null values and keeping the calibration set (26). $\hat{x}_{NO_x f}$ represents the observation of z_{NO_x} by using the adaptive map at every iteration. The adaptive map provides a perfect fitting in about 30 seconds (this might be tuned in order to speed up the estimation by increasing the noise linked to the model but it is not advisable if the sensor model is not perfectly identified). Alternatively, $x_{NO_x f}|_{t=100}$ shows the offline NO_x sensor prediction using the model $\mathbf{\Theta}_{NO_x,\mathbf{100}}$ (table updated after 100 s of running the test) with acceptable results. Finally, $\hat{x}_{NO_x}$ is the online observation of the actual NO_x by using the updating model and the identified bias. This signal should be used for the online NO_x tracking instead of $\hat{x}_{NO_x f}$.

6. Conclusions

In this paper, different possibilities for fusing signals coming from sensors and models are presented by means of applying adaptive filtering. In such sense, diverse adaptive algorithms based on the KF has been designed in order to estimate NO_x in diesel engines and the results are promising. The application of these methods when an on-board NO_x sensor is presented in a turbocharged diesel engine allow to estimate the actual NO_x and update a model in an online basis.

On one hand, the use of look-up tables plus a delayed first order filter for modelling the sensor behavior is presented for estimating NO_x. This simple model is able to reproduce the NO_x emissions in homologation cycles such as the NEDC. On the other hand, different observers are proposed for the online adaptation of the NO_x model presented in part 1 of the paper: the fuel-to-air ratio observation, the online updating of the nominal $NO_{x,0}$ table of the model and a bias

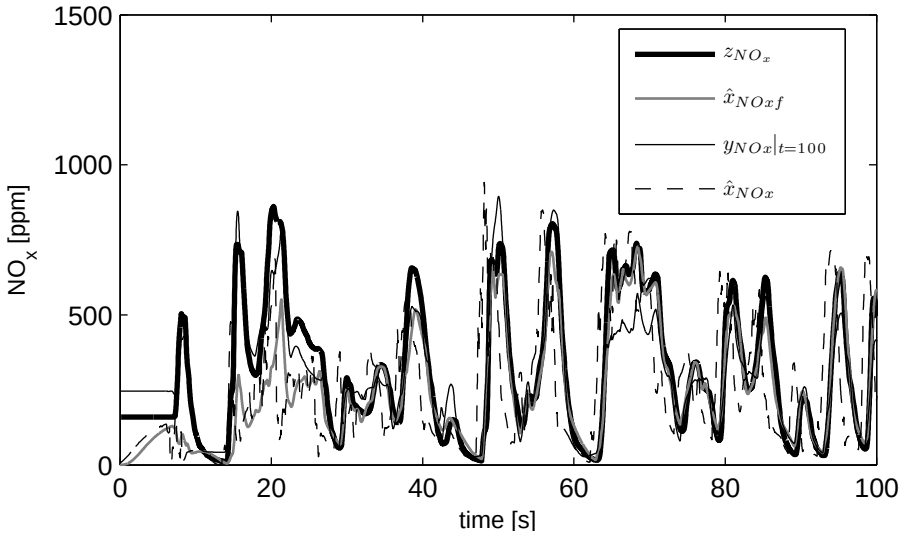

Figure 10: NO_x estimation by three ways: z_{NO_x} sensor measurement, online observation of sensor signal by the SKF method $\hat{x}_{NO_x f}$, offline prediction $y_{NO_x}|_{t=100}$ by using the map $\boldsymbol{\Theta}_{NO_x,\mathbf{100}}$ and the online actual estimation $\hat{x}_{NO_x}$.

model correction. The results show that the model bias can be observed by the online updating of the model parameters and inputs. Finally, the estimation of the actual NO_x by avoiding the delay and sensor filtering is proposed by augmenting the state-space models with the actual signal. This signal is advised for real-time control or diagnosing strategies since it represents the real NO_x emissions and solves the causality problem that exists when measuring on-board, due to sensor delays.

Even though the application to update complex models or much more parameters merits a dedicate analysis to ensure robustness and convergence of the solution, the use of these algorithms seem appropriate to this aim.

[1] EU. Regulation (EC) No 443/2009 of the European Parliament and of the Council of 23 April 2009 setting emission performance standards for new passenger cars as part of the Community's integrated approach to reduce CO_2 emissions from light-duty vehicles. Official Journal of the European Union; 2009.

[2] Guardiola C, Pla B, Blanco-Rodriguez D, Calendini P. ECU oriented models for NO_x prediction. Part 1: A mean value engine model for NO_x prediction. Submitted to Proceedings of the Institution of Mechanical Engineers, Part D: Journal of Automobile Engineering. 2014;.

[3] Rubino L, Bonnel P, Hummel R, Krasenbrink A, Manfredi U, De Santi G. On-road Emissions and Fuel Economy of Light Duty Vehicles using PEMS: Chase-Testing Experimente. SAE Technical Paper 2008-01-1824. 2008;.

[4] Payri F, Luján J, Guardiola C, Pla B. A Challenging Future for the IC Engine: New Technologies and the Control Role. Keynote in ECOSM 2012 Workshop on Engine and Powertrain Control, Simulation and Modeling. 2012;.

[5] Timoney D, Desantes J, Hernndez L, Lyons C. The Development of a Semi-empirical Model for Rapid NO_x Concentration Evaluation Using Measured in-Cylinder Pressure in Diesel Engines. Proceedings of the Institution of Mechanical Engineers, Part D: Journal of Automobile Engineering. 2005;219(5):621–631.

[6] Wahlström J, Eriksson L. Modelling Diesel Engines with a Variable-Geometry Turbocharger and Exhaust Gas Recirculation by Optimization of Model Parameters for Capturing Non-Linear System Dynamics. Proceedings of the Institution of Mechanical Engineers, Part D: Journal of Automobile Engineering. 2011;225(7):960–986.

[7] Kato N, Nakagaki K, Ina N. Thick Film ZrO_2 NO_x Sensor. SAE Technical Paper 960334. 1996;.

[8] Nakanouchi Y, Kurosawa H, Hasei M, Yan Y, Kunimoto A. New Type of NOx Sensors for Automobiles. SAE Technical Paper 961130. 1996;.

[9] Zhuiykov S, Miura N. Development of Zirconia-based Potentiometric NO_x Sensors for Automotive and Energy

Industries in the Early 21st Century: What Are the Prospects for Sensors? Sensors and Actuators B: Chemical. 2007;121(2):639–651.
[10] Galindo J, Serrano J, Guardiola C, Blanco-Rodriguez D, Cuadrado I. An on-engine method for dynamic characterisation of NO_x concentration sensors. Experimental Thermal and Fluid Science. 2011;35(3):470–476.
[11] Faouzi NE, Leung H, Kurian A. Data Fusion in Intelligent Transportation Systems: Progress and Challenges - A Survey. Information Fusion. 2011;12(1):4–10.
[12] Stiller C, Puente Len F, Kruse M. Information Fusion for Automotive Applications - An Overview. Information Fusion. 2011;12(4):244–252.
[13] Schilling A, Amstutz A, Guzzella L. Model-based Detection and Isolation of Faults due to Ageing in the Air and Fuel Paths of Common-rail Direct Injection Diesel Engines Equipped with a λ and a Nitrogen Oxides Sensor. Proceedings of the Institution of Mechanical Engineers, Part D: Journal of Automobile Engineering. 2008;222:101–117.
[14] Kalman R. A New Approach to Linear Filtering and Prediction Problems. Journal of Basic Engineering. 1960;82(35-45).
[15] Alberer D, del Re L. Fast Oxygen based Transient Diesel Engine Operation. SAE Technical Paper 2009-01-0622. 2009;.
[16] Schilling A. Model-Based Detection and Isolation of Faults in the Air and Fuel Paths of Common-Rail DI Diesel Engines Equipped with a Lambda and a Nitrogen Oxides Sensor. ETH-Zürich; 2008.
[17] Höckerdal E, Frisk E, Eriksson L. EKF-based Adaptation of Look-up Tables with an Air Mass-Flow Sensor Application. Control Engineering Practice. 2011;19:442–453.
[18] Höckerdal E, Frisk E, Eriksson L. Observer Design and Model Augmentation for Bias Compensation with a Truck Engine Application. Control Engineering Practice. 2009;17(3):408–417.
[19] Guardiola C, Pla B, Blanco-Rodriguez D, Mazer A, Hayat O. A bias correction method for fast fuel-to-air ratio estimation in diesel engines. Proceedings of the Institution of Mechanical Engineers, Part D: Journal of Automobile Engineering. 2013;227(8):1099–1111.
[20] Guardiola C, Pla B, Blanco-Rodriguez D, Eriksson L. A computationally efficient Kalman filter based estimator for updating look-up tables applied to NO_x estimation in diesel engines. Submitted to Control Engineering Practice. 2013;21(11):1455–1468.
[21] Henningsson M. Data-Rich Multivariable Control of Heavy-Duty Engines. Department of Automatic Control, Lund University, Sweden; 2012.
[22] Galindo J, Luján J, Climent H, Guardiola C. Turbocharging System Design of a Sequentially Turbocharged Diesel Engine by Means of a Wave Action Model. SAE Technical Paper 2007-01-1564. 2007;.
[23] Trimboli S, Di Cairano S, Bemporad A, Kolmanovsky I. Model Predictive Control with Delay Compensation for Air-to-Fuel Ratio Control. vol. 423 of Lecture Notes in Control and Information Sciences. Springer-Verlag Berlin Heidelberg 2012; 2012.
[24] Guardiola C, Pla B, Blanco-Rodriguez D, Cabrera P. A learning algorithm concept for updating look-up tables for automotive applications. Mathematical and Computer Modelling. 2013;57(7-8):1979–1989.
[25] Schilling A, Amstutz A, Onder C, Guzzella L. A Real-Time Model for the Prediction of the NO_x Emissions in DI Diesel Engines. In: Proceedings of the 2006 IEEE International Conference on Control Applications. Munich, Germany; 2006. .
[26] Arrègle J, López J, Guardiola C, Monin C. Sensitivity Study of a NO_x Estimation Model for on-Board Applications. SAE Tecnhical Report 2008-01-0640. 2008;Available from: http://papers.sae.org/2008-01-0640/.
[27] Polni T, Rohal'-Ilkiv B, Alberer D, del Re L, Johansen T. Comparison of Sensor Configurations for Mass Flow Estimation of Turbocharged Diesel Engines. vol. 418 of Lecture Notes in Control and Information Sciences; 2012.

Appendix A. Acronyms

CADC	Common Artemis driving cycle
CO	Carbon monoxide
CO_2	Carbon dioxide
ECU	Electronic control unit
EGR	Exhaust gas recirculation
EKF	Extended Kalman filter
EURO	European emissions standards
FTP	Federal test procedure

HC	Hidrocarbons
KF	Kalman filter
LD	Light duty
LNT	Lean NO_x trap
LS	Least squares
MVEM	Mean value engine model
NEDC	New European driving cycle
NO_x	Nitrogen oxides (NO + NO_2)
O_2	Oxygen
PEMS	Portable emissions measurement system
PM	Particulate matter
RDE	Real driving emissions cycle
RT	Real time
SCR	Selective catalyst reduction
SDMP	Sportive driving mountain profile
SKF	Simplified Kalman filter
SOI	Start of injection
VGT	Variable geometry turbine
WLTC	World light transient cycle
ZrO2	Zirconium oxide (zirconia)

Table A.4: Relevant acronyms used in the paper.

Appendix B. Mathematical symbols

$\dot{m}_a$	Air mass flow	kg/h
$\dot{m}_a^*$	$\dot{m}_a$ set-point reference for controller	kg/h
$\dot{m}_f$	Injected fuel mass flow	kg/h
m_f	Injected fuel mass	mg/str
p_{boost}	Boost pressure	bar
p_{boost}^*	p_{boost} set-point reference for controller	bar
T_{cool}	Engine coolant temperature	K (°C)
p_{int}	Intake pressure	bar
H	Absolute Humidity	%
n	Engine speed	rpm
η_v	Volummetric efficiency	-
z	Sensor measurements	-
x	State-vector	-
u	Input	-
$\hat{x}$	State observation	-
x_r	Actual signal	-
x_f	Filtered signal in order to compare with sensor outputs	
$\boldsymbol{\Theta}$	Adaptive look-up table	-

x_Θ	Output from interpolating the look-up table $\mathbf{\Theta}$	-
K	Kalman gain	-
K_∞	Steady-state Kalman gain	-
σ_w^2	Process variance	-
σ_v^2	Output variance	-
τ	Sensor delay	s (or ms)
	Response time of the sensor	s (or ms)
a	Discrete response time parameter	-
T_s	Sample time	ms
t	time	s
k	Discrete instant	-
z	Z-transform variable	-
$a_{\mathrm{NO_x}}$	Discrete response time of the $\mathrm{NO_x}$ output	-
$\tau_{\mathrm{NO_x}}$	Delay of the $\mathrm{NO_x}$ output	μs
$z_{\mathrm{NO_x}}$	$\mathrm{NO_x}$ output from the $\mathrm{NO_x}$ sensor	ppm
$x_{\mathrm{NO_x}}$	Output from the $\mathrm{NO_x}$ model	g/h (or ppm)
$y_{\mathrm{NO_x}}$	Filtered and delayed output from the $\mathrm{NO_x}$ model	g/h (or ppm)
$x_{\mathrm{NO_x}f}$	Filtered and delayed output from the $\mathrm{NO_x}$ model in the state-space model	g/h (or ppm)
$\hat{x}_{\mathrm{NO_x}}$	Actual $\mathrm{NO_x}$ observation	g/h (or ppm)
$\hat{x}_{\mathrm{NO_x}f}$	Filtered $\mathrm{NO_x}$ observation	g/h (or ppm)
$\theta_{\mathrm{NO_x}}$	Bias on the $\mathrm{NO_x}$ output	g/h (or ppm)
$\hat{\theta}_{\mathrm{NO_x}}$	Observed bias on the $\mathrm{NO_x}$ output	g/h (or ppm)
$\mathbf{\Theta}_{\mathrm{NO_x}}$	Adaptive look-up table for modelling $\mathrm{NO_x}$	g/h (or ppm)
$z_{\lambda^{-1}}$	λ^{-1} output from the $\mathrm{NO_x}$ sensor	-
x_λ^{-1}	λ^{-1} model from the fuel-to-air ratio calculation	-
y_λ^{-1}	Filtered and delayed output from the λ^{-1} model	-
$x_{\lambda^{-1}f}$	Filtered and delayed output from the λ^{-1} model in the state-space model	-
$\hat{x}_{\lambda^{-1}}$	Actual λ^{-1} observation	-
$\hat{x}_{\lambda^{-1}f}$	Filtered λ^{-1} observation	-
$C_{\mathrm{NO_x}}$	Correction factor for $\mathrm{NO_x}$ model	-
C_{dyn}	Dynamic thermal loading factor for $\mathrm{NO_x}$ model	-
k	With subscript: Correction to the $\mathrm{NO_x}$ model	-
C	With subscript: Correction to the $\mathrm{NO_x}$ model	-

Table B.5: Relevant symbols and variables used in the paper.

Appendix C. CADC rural and highway cycles

The common Artemis driving cycles (CADC) are designed upon the basis of an statistical analysis of European real world driving patterns, developed by the European Artemis project (Assessment and Reliability of Transport Emission Models and Inventory Systems). The cycle includes three different variants: urban, rural road and highway. These profiles are more realistic

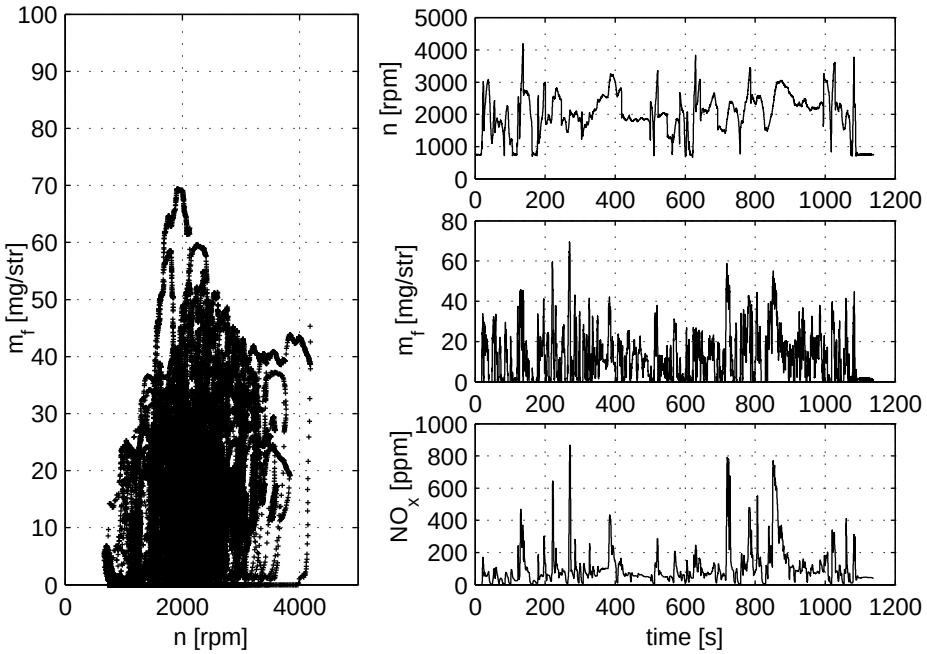

Figure C.11: Rural CADC cycle performed on the engine.

than the NEDC since they cover different real situations and constitute a good source for experimental testing. Rural and highwway versions of the CADC are shown in Figures C.11 and C.12. CADC urban was shown in part 1 of the paper.

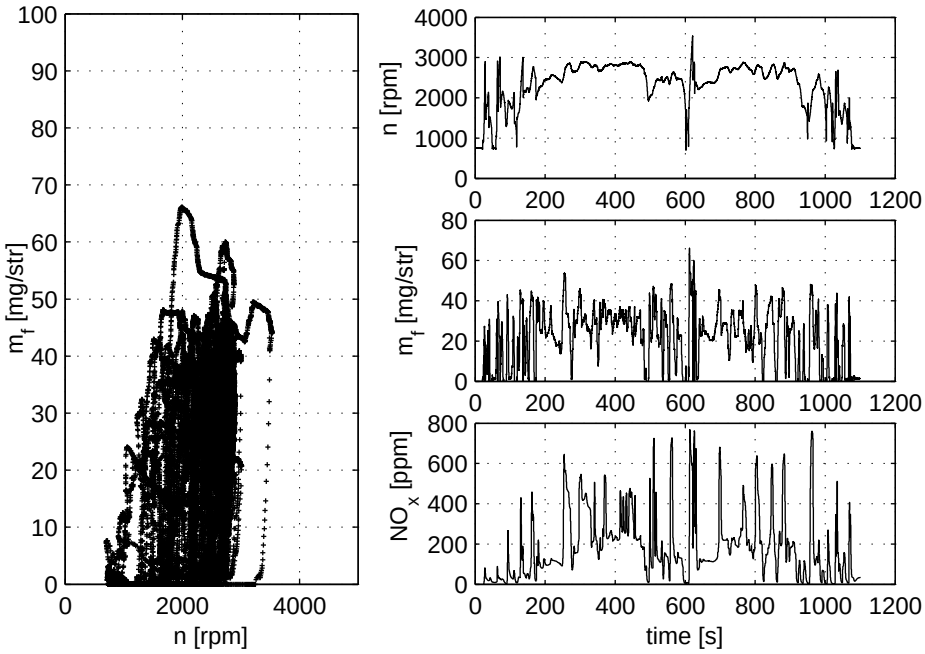

Figure C.12: Highway CADC cycle performed on the engine.